Intermetallic Phase Characteristics in the Mg–Nd–Zn System

Domonkos Tolnai, Samuel A. Hill, Serge Gavras, Tungky Subroto, Ricardo Buzolin, and Norbert Hort

Abstract

Neodymium, a Rare Earth with low solid solubility in Mg is an ideal alloying element to improve the yield strength and creep resistance cost effectively. The addition of Zn achieves a further improvement; however, its influence on the intermetallic phases in the Mg–Nd–Zn ternary system is not yet fully understood. A Mg-5Nd alloy modified with 3, 5 and 7 wt% of Zn was investigated with in situ synchrotron radiation diffraction during cooling from the molten state to 200 °C in order to investigate the phase-formation and -transformation characteristics of the alloys. The synchrotron diffraction results have been complemented with TEM investigations on the as-solidified samples. The results suggest that Zn has a strong effect on the microstructure by stabilizing the Mg_3Nd phase and accelerating the precipitation formation. The experimental results do not fully comply with the theoretical calculations, indicating the necessity of improving the thermodynamic databank for this alloy system.

Keywords

Mg–Nd–Zn alloys • Intermetallic phases • In situ synchrotron diffraction • Solidification

Introduction

The constant strive on energy efficiency has increased the importance of weight saving through light-weight design in the automotive and aerospace industries [1]. The high specific strength and stiffness of Mg and its alloys [2] complemented by their generally good castability would ensure a prominent place among the materials used for transportation. Despite their advantages, the wide usage is hindered by their poor absolute properties, insufficient formability at ambient temperatures [3] and weak corrosion resistance. The latter, however can be exploited in the field of degradable implant development [4].

There are two approaches to improve the poor absolute strength of Mg; generating secondary phases with reinforcing characteristics and/or thermo-mechanical processing to obtain ultrafine structures. An effective solution to enhance the mechanical property profile of Mg is the alloying with the combination of Zn and Rare Earth (RE) metals [5]. The addition of Zn to the Mg–RE systems accelerates the age hardening response and increases the peak strength due to the uniformly distributed basal precipitates [6,7]. The addition of RE improves the castability further and increases the elevated temperature strength [8]. Furthermore, it weakens the anisotropy [9, 10] that leads to improved ductility of Mg alloys.

These alloys are produced mainly in the form of castings therefore their property profile is determined during the solidification [11, 12] and the following thermo-mechanical processing [13]. Thus, controlling the sequence of formation and evolution of the meta-stable and stable phases during solidification is a prerequisite to the design of the microstructure.

Performing in situ diffraction experiments while cooling the molten sample to the fully solidified state, allows identifying the secondary phases, to determine their solidification sequence [14, 15] and to use these results for experimental validation of the existing thermodynamic databases on the investigated system.

D. Tolnai (✉) · S. A. Hill · S. Gavras · T. Subroto · R. Buzolin · N. Hort
Magnesium Innovation Centre, Helmholtz-Zentrum Geesthacht, Max-Planck Str. 1, Geesthacht, D21502, Germany
e-mail: domonkos.tolnai@hzg.de

S. A. Hill
Department of Materials Science & Metallurgy, University of Cambridge, 27 Charles Babbage Rd, Cambridge, CB30FS, UK

R. Buzolin
Institue of Materials Science, Joining and Forming, Graz University of Technology, Kopernikusgasse 24/I, 8010 Graz, Austria

D. Orlov et al. (eds.), *Magnesium Technology 2018*, The Minerals, Metals & Materials Series, https://doi.org/10.1007/978-3-319-72332-7_61

Experimental Methods

The alloys were prepared by permanent mould indirect chill casting [16]. Pure Mg was melted in an electric resistance furnace under protective atmosphere of 2 vol.% SF_6 and Ar. The Zn and Nd alloying elements were added as pure materials. After mixing, the melt was held at 720 °C for 10 min then was poured into a steel mould preheated to 660 °C. After 5 min isothermal holding the mould was quenched into water at a rate of 10 mm s^{-1} until the top of the melt was in line with the cooling water level. The composition of the ingots was measured by Spark Optical Emission Spectroscopy and X-ray Fluorescence Spectroscopy.

The metallographic preparation of the samples was done by grinding using SiC paper and polishing with OPS solution. For the optical microscopy (OM) investigation the samples were etched with acetic-picral solution. The OM analyses were performed using a Leica DMI 500 light optical microscope. The average grain size was calculated based on measuring 100 grains using the line intercept method.

Scanning Electron Microscopy (SEM) was done with a Tescan Vega 3 SEM. A Phillips CM200 Transmission Electron Microscope (TEM) with accelerating voltage of 200 kV was used to obtain bright field (BF) micrographs and microbeam selected area diffraction (SAED) patterns of the intermetallic phases. TEM foils were prepared via electropolishing using a 1.5% perchloric acid solution in ethanol.

In situ solidification synchrotron diffraction experiments were performed at the P07 (HEMS) beamline of PETRA III at DESY (Deutsches Elektronen-Synchrotron). A monochromatic beam with a cross-section of 1.1 mm 1.1 mm was used, and a beam energy of 100 keV (λ = 0.0124 nm) was used. The acquisition time for each image was 0.5 s. The samples were encapsulated in stainless steel crucibles under Ar atmosphere. The experiments were performed in the chamber of a modified DIL805 A/D dilatometer (Bähr-Thermoanalyse GmbH, Hüllhorst, Germany). The diffraction patterns were acquired with a PerkinElmer 1622 Flatpanel detector with pixel size of $(200\ \mu m)^2$ The distance between sample and detector was 1603 mm (calibrated with a LaB_6 standard powder sample). The sample was heated to 800 °C with a then held at this temperature for 5 min before cooling to room temperature with a cooling rate of 50 K/min. The recorded diffraction patterns were analyzed using Fit2D.

Solution treatments were performed at 460 °C for 24 h in an electric resistance furnace and were immediately followed by room temperature water quenching. Samples were solution treated. Ageing treatments were performed at 250 °C for 168 h and were immediately followed by room temperature water quenching.

For the hardness measurements samples were ground using SiC paper up to P2500 before testing. The vickers hardness (HV5/30) was measured on an EMCO TEST M1C 010 hardness machine using 5 kg with a loading time of 30 s. 10 indentations were taken per sample.

Phase diagrams were produced with PANDAT^{TM} 2016.1 software using the PanMg 2017 database. The Nd content was set to 4.3 wt%. A diagram was constructed with no suppressed phases, and one with the phases $Mg_{41}Nd_5$ and $Mg_{12}Nd$ suppressed.

Results and Discussion

The actual alloy compositions measured with spark analyser and XRF are listed in Table 1.

As-Cast Microstructure

The as-cast microstructures of the investigated alloys are shown in Fig. 1a–c. In all the alloys, there is a semi-continuous network of intermetallic particles at the grain boundaries. The grain sizes are measured on optical metallographic images as 0.56 ± 0.03 mm for Mg5Nd3Zn, 0.36 ± 0.02 mm for Mg5Nd5Zn and 0.2 ± 0.02 mm for Mg5Nd7Zn, respectively.

To analyse the influence of Zn additions on the volume fraction and morphology of the intermetallic phases, SEM investigations were used (Table 2).

In all the alloys two types of intermetallic phases are present, a eutectic lamellar and a continuous intermetallic morphology. The latter has an increasing volume fraction as the Zn content is increased to 5 wt% and further to 7 wt% as shown in Fig. 1.

Table 1 Chemical composition of the alloys

Composition	Nd wt%(XRF)	Zn wt%(spark)
Mg5Nd3Zn	4.35	3.20
Mg5Nd5Zn	4.20	5.20
Mg5Nd7Zn	4.34	8.00

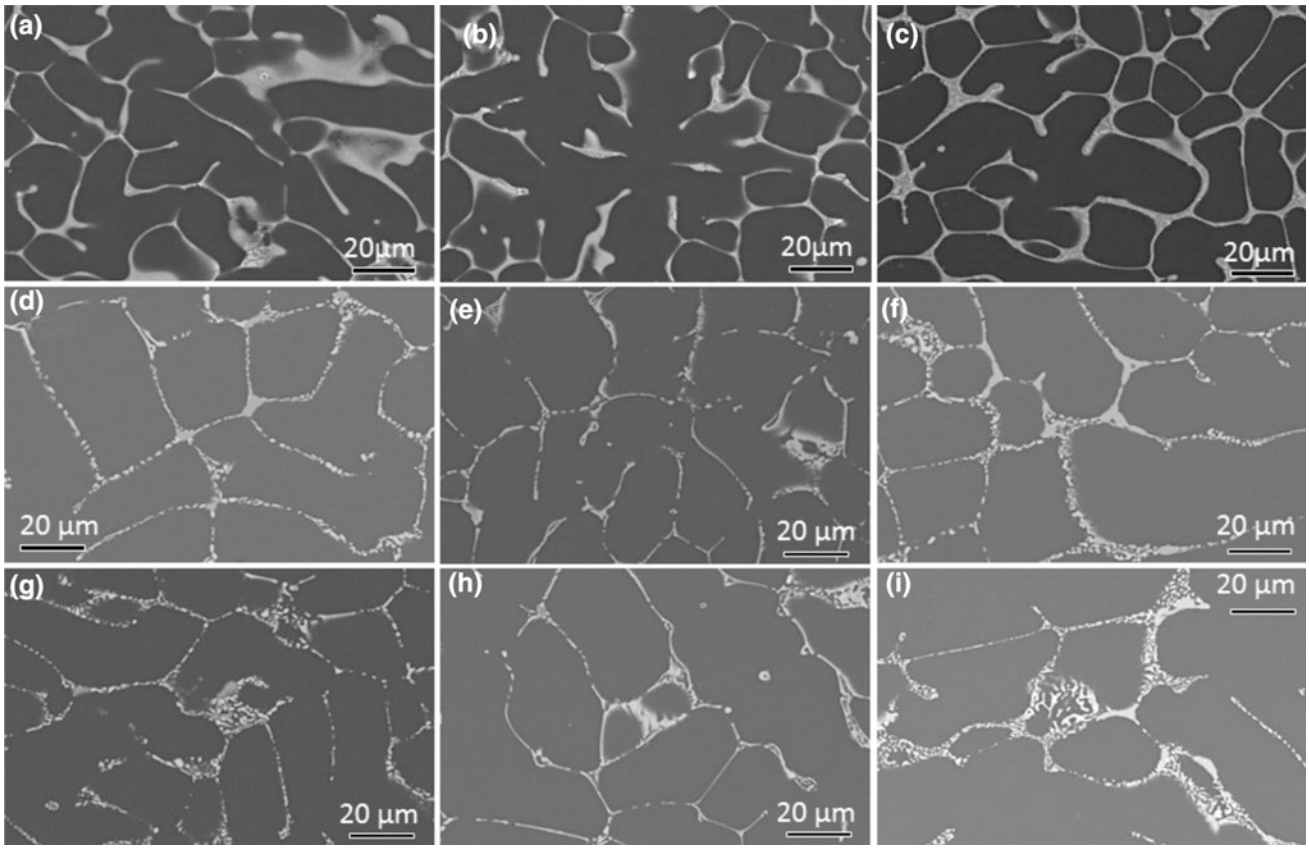

Fig. 1 SEM micrographs of Mg5Nd3Zn (**a**, **d**, **g**) Mg5Nd5Zn (**b**, **e**, **h**) and Mg5Nd7Zn (**c**, **f**, **i**) in as-cast (**a–c**), solution heat treated (**d–f**), and aged (**g–i**) conditions

Table 2 Average volume fraction of the intermetallic phase in the investigated alloys

Composition (wt%)	Average volume fraction (%)
Mg5Nd3Zn	13.9 (± 1.7)
Mg5Nd5Zn	13.4 (± 0.4)
Mg5Nd7Zn	15.2 (± 0.7)

Phase Identification

In order to characterize the intermetallic phases, synchrotron radiation diffraction was used. The line profiles of the samples in as-cast condition are shown in Fig. 2.

The results show that in the case of Mg5Nd3Zn only one intermetallic, the Mg_3(Nd, Zn) quasi binary phase is present. Although on the SEM images two distinct phases are observed, it is possible that the continuous morphology has such a low volume fraction that is below the detection limit of the synchrotron diffraction. In the case of the higher Zn containing alloys the $Mg_{50}Nd_8Zn_{42}$ phase is clearly detectable. To support the results of the synchrotron radiation diffraction investigations, TEM phase identification was performed on the intermetallic particles. Using micro-beam electron diffraction, it was possible to obtain selected area electron diffraction patterns from the intermetallic phases. Following zone axis identification, it was confirmed that the intermetallic lamellar phase was quasi-binary face-centred cubic (FCC) phase, Mg_3(Zn, Nd) while the continuous intermetallic phase was a c-centered orthorhombic phase $Mg_{50}Nd_8Zn_{42}$. Figure 3 shows a region of the sample from Mg5Nd5Zn, where these two different intermetallics lie adjacent to each other.

Thermal Analysis

Differential Thermal Analysis (DTA) was used to obtain the liquidus and solidus temperatures of the alloys. The samples were subjected to three subsequent heating-cooling cycles with a rate of 10 K/min. The results show that with the increasing Zn content the formation temperatures of the phases decrease and the freezing range increases as shown in Table 3.

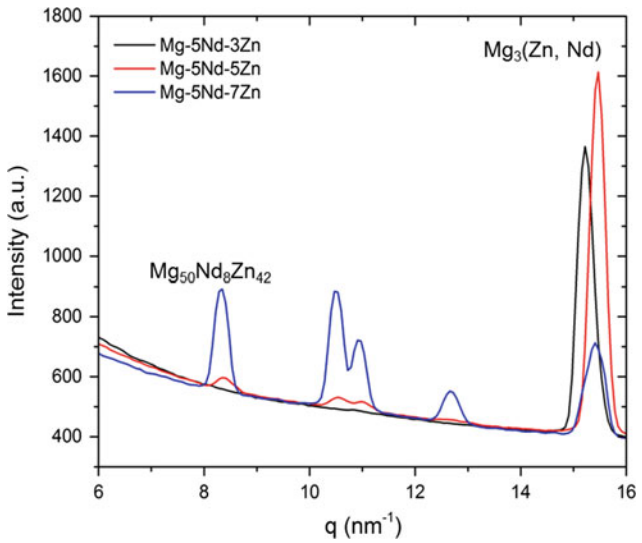

Fig. 2 Section of the line profiles of the investigated Mg–Nd–Zn alloys

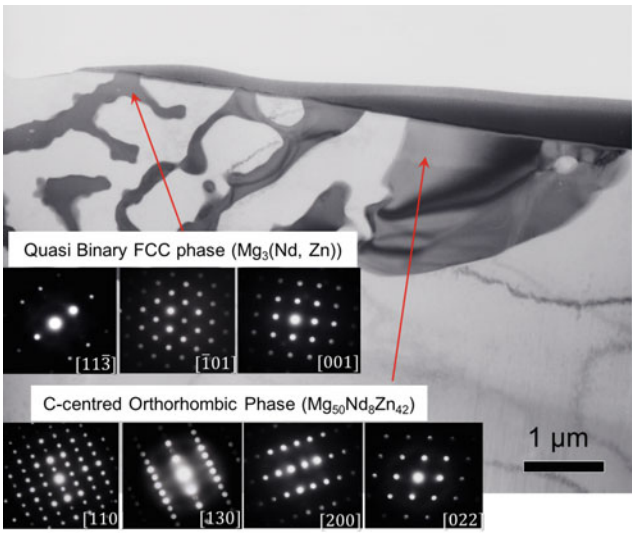

Fig. 3 Mg5Nd5Zn bright field micrograph of showing 2 adjacent intermetallic phases the lamellar FCC and the continuous intermetallic with c-centred orthorhombic phase with corresponding zones axes showed respectively

Table 3 Liquidus and solidus temperatures measured with DTA and phase formation temperatures measured by in situ synchrotron diffraction at 50 K/min cooling rate

	Mg5Nd3Zn	Mg5Nd5Zn	Mg5Nd7Zn
Liquidus (°C)	628	623	616
Solidus (°C)	510	495	487
α-Mg (°C)	633	633	623
Mg_3(Nd, Zn) (°C)	511	508	488
$Mg_{50}Nd_8Zn_{42}$ (°C)	N/A	462	469

Table 4 Changes in Vickers hardness through heat treatment

	As-cast	Solution treated	Aged
Mg5Nd3Zn	57.4 ± 4.5	42.9 ± 3	40.3 ± 2
Mg5Nd5Zn	50.3 ± 3	42.6 ± 3.4	43 ± 3.4
Mg5Nd7Zn	65.1 ± 3.9	48.6 ± 3.7	51.7 ± 2.9

In situ synchrotron diffraction experiments were performed during melting and subsequent cooling of the samples in order to investigate the solidification sequence of the alloys and to determine whether phase transformations occur in liquid or solid state. The results indicate that first α-Mg dendrites form followed by the Mg_3(Nd, Zn) quasi binary phase. The solidification ends with the formation of $Mg_{50}Nd_8Zn_{42}$ phase detected only in the higher Zn containing alloys, Mg5Nd5Zn and −7Zn as shown in Fig. 4.

During the post mortem metallographic investigation of the as-solidified samples from the in situ solidification experiments, precipitations were found in the matrix as shown in Fig. 5. From the initial investigation of these precipitates, it is likely that they are Mg_3RE (Mg_3Nd in this investigation). However, further analysis needs to be completed before the phase of the precipitates can be decisively stated. The presence of precipitates may be explained by the reduction in solubility within the hcp matrix upon cooling. The final solid hcp Mg will likely form with the maximum solid solubility of Nd and Zn. This coring effect would explain the tendency of precipitates to form close to the intermetallics on the grain boundaries, as these are regions of greater solute enrichment.

Heat Treatments

The evolution of the microstructure through solution heat treatment and ageing is shown in Fig. 1d, e, f, g, h, i, respectively. The volume fraction of intermetallics decreases during solution treatment as they dissolved into solid solution in the α-Mg matrix. SEM micrographs show both intermetallic phases present in Mg5Nd3Zn (Fig. 1d) and in Mg5Nd7Zn (Fig. 1f). The Mg5Nd5Zn alloy is likely to

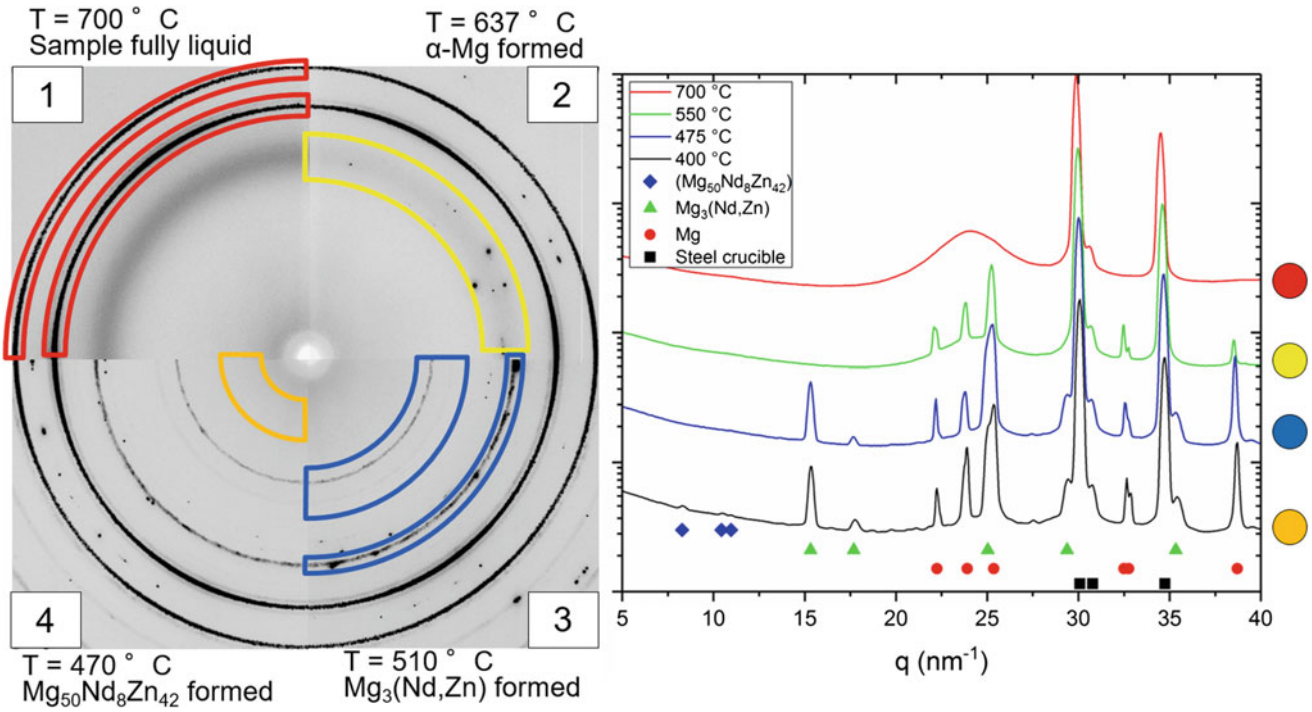

Fig. 4 Solidification sequence of Mg5Nd5Zn, obtained by in situ synchrotron radiation diffraction

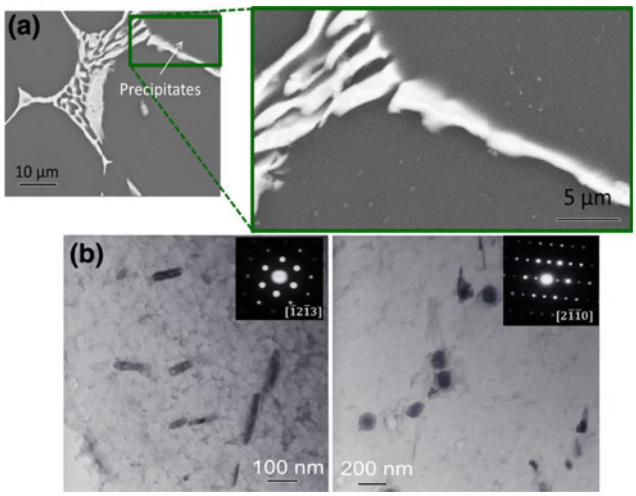

Fig. 5 **a** SEM BSE micrograph overview of Mg5Nd3Zn following melting and solidification at 100 K/min indicating the location of precipitates **b** TEM BF Mg_3RE precipitates from two different zone axes present following melting and solidification at 100 K/min in Mg5Nd5Zn

contain both intermetallic phases, but only the quasi-binary phase is evident in Fig. 1e.

Micrographs show the continuous phase to form a different shape after the solution heat treatment. The quasi-binary phase appears to form between successive dendrite arms, whereas the continuous phase is likely to be located between successive dendrites, or in larger voids. 2D micrographs show this as the quasi-binary phase linking the continuous regions. Precipitates were observed in all microstructures after ageing. They appear to be more evenly distributed. This is as expected, as the heat treatments allow diffusion within the matrix, leading to a more even solute distribution. They are seen to form arrays, likely along defects such as a dislocation. With increasing Zn content the precipitates appear to become finer.

The change in Vickers hardness of the alloys throughout the heat treatments is shown in Table 4.

In case of all three alloys a decrease in hardness can be observed after solution heat treatment. Although intermetallic particles precipitate, there are no significant differences between the solution treated and the aged samples. The T6 heat treatment is seen to decrease the hardness of all alloys, indicating that such a high alloying content is already detrimental to the age hardening of the system [17]. In this case the hardness is not strongly dependant on the precipitation strengthening, instead relies on the volume fraction of the intermetallic phases. These hard particles can effectively strengthen the matrix, and as during the heat treatment their volume fraction decreases their overall strengthening capability shows the same trend.

Thermodynamic Modeling

A quasi-binary section of the Mg–Nd–Zn phase diagram at 4.3 wt% Nd content calculated with Pandat is shown in Fig. 6.

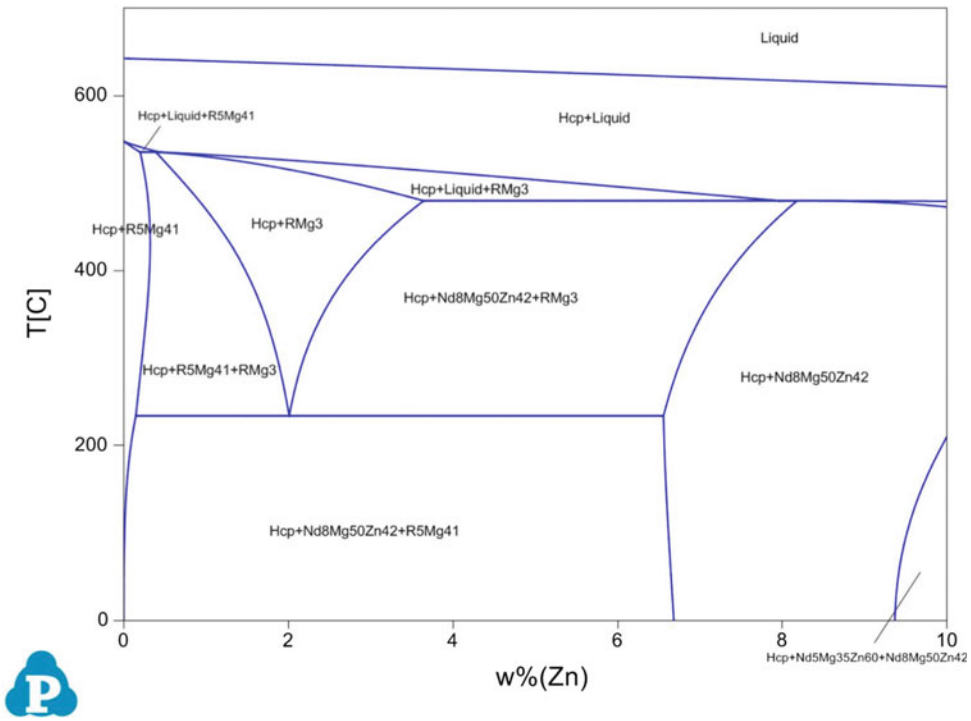

Fig. 6 Quasi-binary section of the Mg–Nd–Zn phase diagram at 4.3 wt% Nd

It is evident that the equilibrium phase diagram cannot describe the reality in this case. However, the continuous intermetallic phase ($Mg_{50}Nd_8Zn_{42}$) is predicted in the case of all alloys, the investigations did not reveal the presence of $Mg_{41}Nd_5$, which is reported to be the stable phase in Mg–Nd binary system. When the simulation is performed with the $Mg_{41}Nd_5$ phase suppressed, $Mg_{12}Nd$ is predicted instead, which is in good correlation with previous findings under realistic solidification conditions [15]. Suppressing this phase as well, leads to the correct description of the phases as shown in Fig. 7.

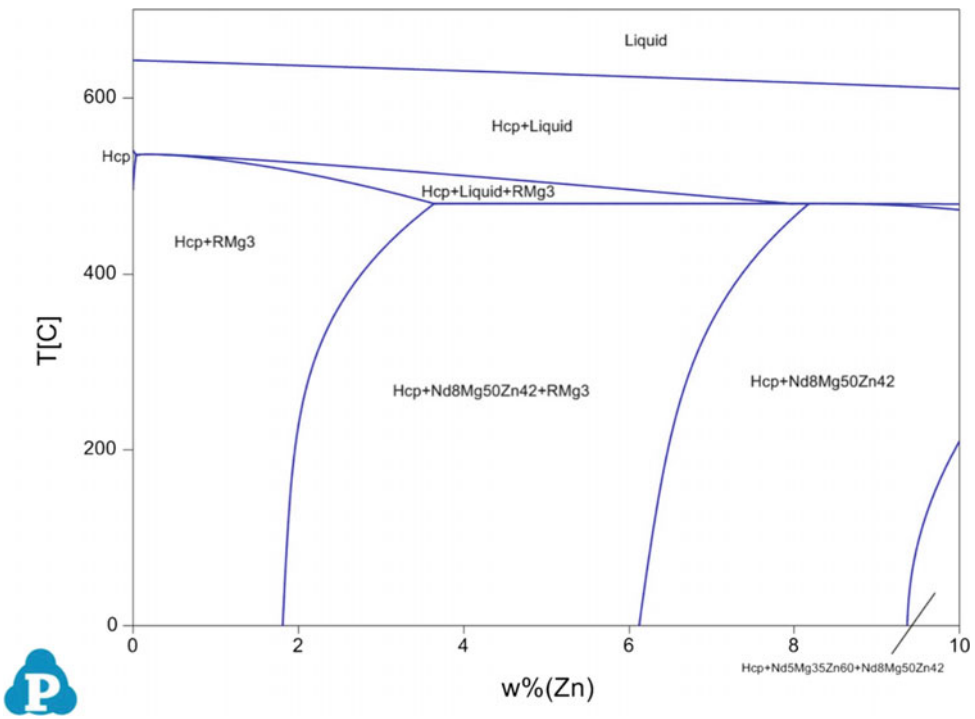

Fig. 7 Quasi-binary section of the Mg–Nd–Zn phase diagram at 4.3 wt% Nd excluding the $Mg_{41}Nd_5$ and $Mg_{12}Nd$ phases

However, the latter thermodynamic calculation yields good result in the case of the lower Zn content alloys, the description of Mg4NdZn8 (Mg5Nd7Zn) is still incorrect, since it does not predict the Mg_3(Zn, Nd) phase. This suggests, the necessity of improving the corresponding thermodynamic database.

Conclusions

From the phase identification and thermal-analyses of the alloys from the Mg–Nd–Zn system the following conclusions can be drawn:

- The increasing Zn content decreasing the grain size of the alloys.
- There are two different intermetallic phases present in the alloys, the face centered cubic Mg_3(Nd, Zn) and the c centered orthorhombic $Mg_{50}Nd_8Zn_{42}$ phase. The latter has a negligible volume fraction in the lowest Zn content Mg5Nd3Zn alloy.
- Precipitation have been found in the as-solidified samples, close to the grain boundaries and the intermetallic phases. This can be a result of solute enrichment of these regions during solidification.
- The solution and ageing heat-treatments lead to the worsening of the hardness, indicating that precipitation strengthening has no decisive effect on the overall strength of the material.
- The addition of Zn to binary Mg-Nd alloys stabilizes the Mg_3(Nd, Zn) phase.
- The thermodynamic databases not correlate with the experimental results, however in the case of Mg5Nd3Zn and -5Zn the calculations give acceptable results when the $Mg_{41}Nd_5$ and the $Mg_{12}Nd$ phases are suppressed.

Acknowledgements The authors acknowledge the Deutsches Elektronen-Synchrotron for the provision of facilities within the framework of the proposal I-20150471 and the Deutsche Forschungsgemeinschaft for the funding in the framework of the proposals TO817/4-1 and ME4487/1-1.

References

1. M. Pekguleryuz, K. Kainer, A. Kaya, Fundamentals of magnesium alloy metallurgy, first ed. Woodhead, Philadelphia, 2013.
2. M.M. Avedesian, H. Baker, Magnesium and magnesium alloys, ASM Speciality Handbook, ASM International, United States of America, 1999.
3. M.H. Yoo, J.R. Morris, K.M. Ho, S.R. Agnew, Metall. Mater. Trans. A 41 (2002) 813–822.
4. H. Hermawan, D. Dubé, D. Mantovani, "Developments in metallic biodegradable stents" Acta Biomaterialia 6 (2010) 1693–1697.
5. T. Itoi et al.: Microstructure and mechanical properties of Mg-Zn-Y alloy sheet prepared by hot-rolling, Mater Sci Eng A, 560 (2013) 216–223.
6. J. F. Nie et al.: Enhanced age hardening response and creep resistance of Mg–Gd alloys containing Zn: Scr. Mater., 53, (2005) 1049–1053.
7. T. T. Sasaki et al.: Enhanced age hardening response by the addition of Zn in Mg–Sn alloys, Scripta. Mater., 55, (2006). 251–254.
8. Q. Li, et al.: Effect of Nd and Y addition on microstructure and mechanical properties of as-cast Mg–Zn–Zr alloy, J. Alloys Compd., 427, (2007) 115–123.
9. N. Stanford et al.: Effect of microalloying with rare-earth elements on the texture of extruded magnesium-based alloys Scripta. Mater., 59, (2008) 772–775.
10. B. Langelier et al.: Improving microstructure and ductility in the Mg–Zn alloy system by combinational Ce–Ca microalloyingMat. Sci. Eng. A, 620, (2015) 76–84.
11. D. Tolnai et al., "In situ synchrotron tomographic investigation of the solidification of an AlMg4.7Si8 alloy" Acta Materialia 60 (2012) 2568–2577.
12. S. Terzi et al., "In situ study of nucleation and growth of the irregular α-Al/β-Al_5FeSi eutectic by 3-D synchrotron X-ray microtomography" Acta Materialia 58 (2010) 5370–5380.
13. D. Tolnai et al., "Sub-micrometre holotomographic characterisation of the effects of solution heat treatment on an AlMg7.3Si3.5 alloy" Materials Science and Engineering A 550 (2012) 214–221.
14. O. Shuleshova et al., "In situ observations of solidification in Ti–Al–Ta alloys by synchrotron radiation" Intermetallics 19 (2011) 688–692.
15. D. Tolnai et al., "In situ synchrotron diffraction of the solidification of Mg4Y3Nd" Materials Letters 102–103 (2013) 62-64.
16. F.R. Elsayed et al., Magnesium permanent mold Castings optimization Materials Science Forum 690 (2011) 65–68.
17. J.F. Nie, "Precipitation and hardening in magnesium alloys" Metallurgical and Materials Transactions A 43(11) (2012) 3891–3939.